

Flow-Induced Noise of a Forward-Backward Facing Step

Matthias Springer, Christoph Scheit and Stefan Becker

Abstract This work deals with the aeroacoustic sound radiated by a forward-backward facing step. A large eddy simulation with coupled aeroacoustic computation was carried out. In addition, acoustic measurements in an acoustic wind tunnel were conducted and compared with the numerical results. The sound radiation of the step geometry is dominated by broadband noise. The results show that the simulation is able to capture the acoustic field and the numerical results enable the identification of flow regions responsible for sound generation.

1 Introduction

Flow induced noise plays an important role in many technical applications. As an example, the noise generated by the flow field around cars or planes has an unfavorable influence on the comfort for passengers and therefore on the quality of the vehicle. In order to predict the acoustic behavior of technical products during the design process, the usage of numerical simulation software is a valuable measure to prevent unfavorable acoustic effects. Flow noise is induced by turbulent pressure fluctuations. For the present investigations, a forward-backward facing step is used as a simplified geometry. Broadband noise is emitted from this geometry. Previous studies dealing with this geometry are shown in [1]. Here, a large eddy simulation (LES) in the context of Fluid-Structure-Acoustic Interaction is shown. In this work, the aeroacoustic noise was overpredicted compared to measurements. Another work dealing with a forward-backward facing step geometry is published in [2]. It deals with an elongated step geometry. Acoustic source terms for the linearized euler equations are generated based on a flow field computed with means of LES. Aeroacoustic results are shown only qualitatively here. In [3], the sound radiation of a forward

M. Springer (✉) · C. Scheit · S. Becker
Institute of Process Machinery and Systems Engineering, University Erlangen-Nuremberg,
Cauerstraße 4, 91058 Erlangen, Germany
e-mail: sp@ipat.uni-erlangen.de
URL: <http://www.ipat.uni-erlangen.de/>

© Springer International Publishing Switzerland 2016
A. Dillmann et al. (eds.), *New Results in Numerical and Experimental Fluid Mechanics X*, Notes on Numerical Fluid Mechanics and Multidisciplinary Design 132, DOI 10.1007/978-3-319-27279-5_67

767

facing step based on linearized perturbed compressible equations is shown. Comparisons with experiments show good coincidence.

In the current work, the aeroacoustic field generated by the turbulent flow around the step is the result of a coupled computation between flow field and acoustic field. The coupling between the two physical fields is realized by the generation of acoustic source terms based on the turbulent flow field. To account for the noise inducing pressure fluctuations, a scale resolving flow computation at a Reynolds number in the range of technical applications was carried out. At simulation time, aeroacoustic source terms were computed from the velocity field data. In a post processing step, the acoustic field is computed on the basis of the acoustic source terms. Besides the numerical investigations, measurements were conducted to assess the computed results. Microphone measurements of the sound radiated by the forward-backward facing step were carried out in a low-noise wind tunnel. A comparison between numerical and experimental results will be given and discussed.

2 Numerical Setup

The three-dimensional flow field generated flow by the forward-backward facing step was computed by means of LES. The flow computation was carried out using the software FASTEST-3D [4]. This code solves the transient, incompressible Navier-Stokes equations for newtonian fluids on structured grids.

The equations are discretised using the finite volume method (FVM). The influence of the unresolved flow scales was modeled with a Smagorinsky subgrid scale model. The Smagorinsky constant was chosen to be 0.1. Time discretisation was performed with a 4th-order Runge-Kutta Scheme. For the calculation of the convective fluxes, a Central Difference Scheme was used. The velocity-pressure coupling is conducted with the Predictor-Corrector algorithm.

The forward-backward facing step is a quadratic obstacle attached on a flat plate with edge length of $D = 20$ mm. The spanwise extend of the geometry was chosen to be $5D$. In spanwise direction, periodic boundary conditions were applied. The height of the computational domain was $20D$. At the inflow boundary, a laminar boundary layer profile was set. This boundary layer profile origins from LDA-measurements during previous performed experimental investigations [1] of the current geometry. The velocity at the boundary layer edge was 20 m/s. This yields a Reynolds number of 26.000, based on inflow velocity and step height D . The grid size was chosen to get a wall normal resolution of $y^+ < 1$ (Fig. 1b). The streamwise and spanwise resolution in the wake region of the step was $x^+ < 40$ (Fig. 1a) and $z^+ < 20$ (Fig. 1c), respectively. The overall number of hexahedron control volumes was 91.6 Millions. To get a CFL-number below 1, the time step size was chosen to be $4 \cdot 10^{-7}$ s.

Acoustic source terms were computed at simulation time from the incompressible flow variables. Based on these acoustic source terms, the radiation of sound was computed with the software CFS++ [5]. This solver uses the finite element method (FEM) to solve the Lighthill equation.

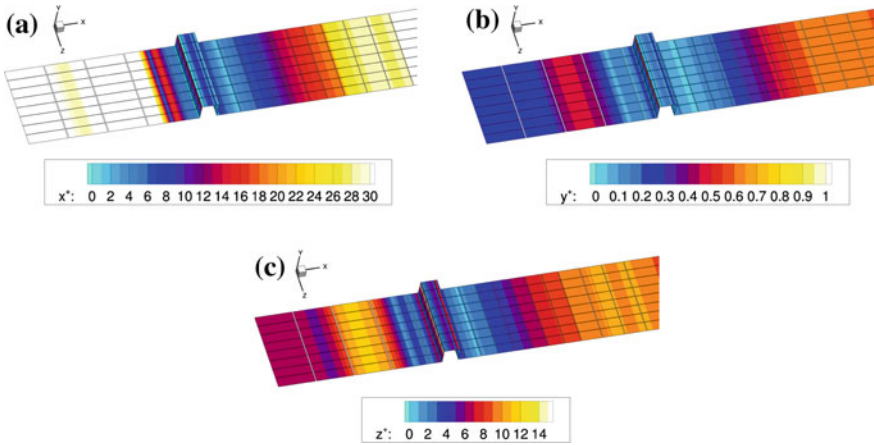


Fig. 1 Time averaged distribution of x^+ , y^+ and z^+ . **a** Time averaged x^+ - distribution, **b** time averaged y^+ - distribution, **c** time averaged z^+ - distribution

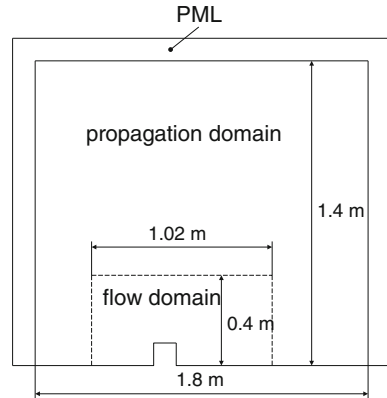
$$\frac{\partial^2 \rho}{\partial t^2} - c_0^2 \frac{\partial^2 \rho}{\partial x_i^2} = \frac{\partial^2 T_{ij}}{\partial x_i \partial x_j} \quad \text{with} \quad T_{ij} \approx \rho_0 u_i u_j \tag{1}$$

The Lighthill Tensor is denoted by T_{ij} . In the present work an alternative source term formulation, which is equivalent to the original formulation, is used. Taken the divergence of the incompressible momentum equations for newtonian fluids, one gets:

$$\frac{\partial^2 (\rho_0 u_i u_i)}{\partial x_i \partial x_j} = - \frac{\partial^2 p}{\partial x_i^2} \tag{2}$$

Using this formulation as right-hand side for Lighthill’s acoustic analogy, the acoustic pressure is computed for a region shown in Fig. 2. The spanwise extent of the propagation region is equal to the spanwise extent of the flow region. Except the walls of the fluid domain, the whole acoustic domain is surrounded by a perfectly matched layer (PML [6]) in order to damp the acoustic pressure to zero towards the outer faces of the domain. Thereby reflections of acoustic waves at the domain boundaries can be prevented.

Acoustic source terms are calculated at simulation time during flow computation [7]. The source terms are stored on the CFD grid. The acoustic computation is performed on a grid which is much coarser than the CFD grid. Therefore, a conservative interpolation between the fine CFD grid and the much coarser CAA grid has to be done [8]. The CAA grid is an equidistant, orthogonal, hexahedral grid with a grid size of 5 mm in streamwise and wall-normal direction. Due to this grid size, acoustic waves until approximately 3300 Hz are resolved spatially with 20 computational points per wavelength. The grid size in spanwise direction is 10 mm. The output

Fig. 2 Acoustic domain

interval for acoustic source terms is $4 \cdot 10^{-5}$ s (sampling rate 25 kHz). Acoustic waves with frequency up to 2500 Hz are resolved with 10 points per period. A physical time period of 0.133 s was realized.

3 Experimental Setup

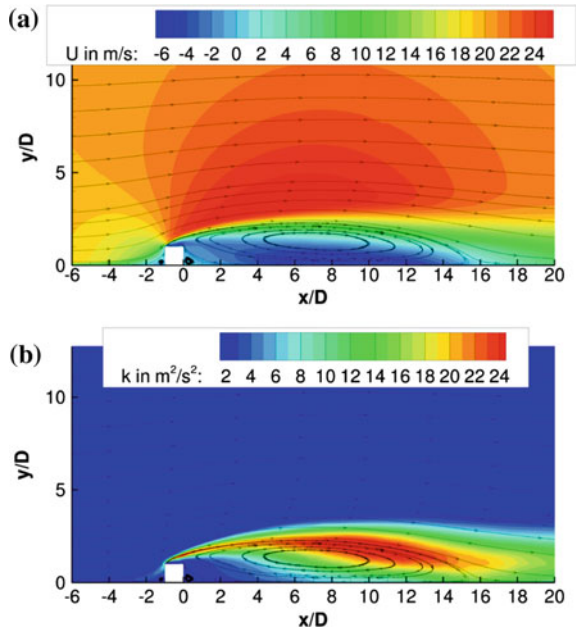
The acoustic measurements were performed in the acoustic wind tunnel of the University of Erlangen–Nuremberg, which is equipped with sound absorbers (anechoic chamber conditions). A description of the wind tunnel is given in [9]. The square cylinder obstacle with edge length of $D = 20$ mm was attached on a flat plate. The spanwise extent of the obstacle was $35 D$. The measurements were carried out at 20 and 30 m/s. In the case of 20 m/s, the same Reynolds number as in the simulation was realized. The simulated results show that the laminar boundary layer of the inflow became rapidly turbulent because a turbulent boundary layer profile starts to develop at $0.5D$ after the inlet. Therefore a boundary layer tripping was installed right after the wind tunnels nozzle to ensure comparable boundary conditions between measurement and simulation. A microphone was installed directly above the step with a distance of 1 m. The microphone measurements were performed for 30 s with a sampling rate of 48 kHz. The microphones used were $1/2$ –inch free-field microphones from Bruel & Kjaer from the type 4189 – L – 001.

4 Results

4.1 Flow Field

The time-averaged flow field generated by the forward-backward facing step is shown in Fig. 3a. The flow is characterised in principle by two recirculation areas. The first

Fig. 3 Time-averaged velocity field and distribution of turbulent kinetic energy k . **a** time-averaged velocity field in main flow direction, **b** time-averaged k -distribution



recirculation area develops in front of the obstacle due to pressure induced boundary layer separation. Its length is $1.6D$. The second recirculation area is formed by the wake of the obstacle. It has a length of $16.2D$. In Fig. 3b the time-averaged distribution of the turbulent kinetic energy is shown. Turbulence develops mainly in the shear layers between the main flow and the recirculation areas. Due to the large velocity gradients in the shear layer of the rear recirculation area, especially behind the obstacle’s windward edge, the maxima of the turbulent kinetic energy are located there.

LDA measurements [1] show comparable size of the front recirculation area, but a much shorter detachment length of the rear recirculation area. The measured detachment length is $10.5D$. These differences can be explained with the spanwise extent of the flow domain. The chosen extent of $5D$ is not sufficient to let the spanwise velocity correlations drop to zero. Nevertheless, profiles of the turbulent kinetic energy (Fig. 4) are comparable to the LDA measurements. The shape, as well as the peak values are very similar. Due to the larger extent of the rear recirculation area in case of the simulation, the location of the maximum of the turbulent kinetic energy is above the maximum of the measured values.

4.2 Aeroacoustic Simulation

The aeroacoustic computation using Lighthill’s acoustic analogy is based on the acoustic source term distribution. In Fig. 5, the distribution of the source term den-

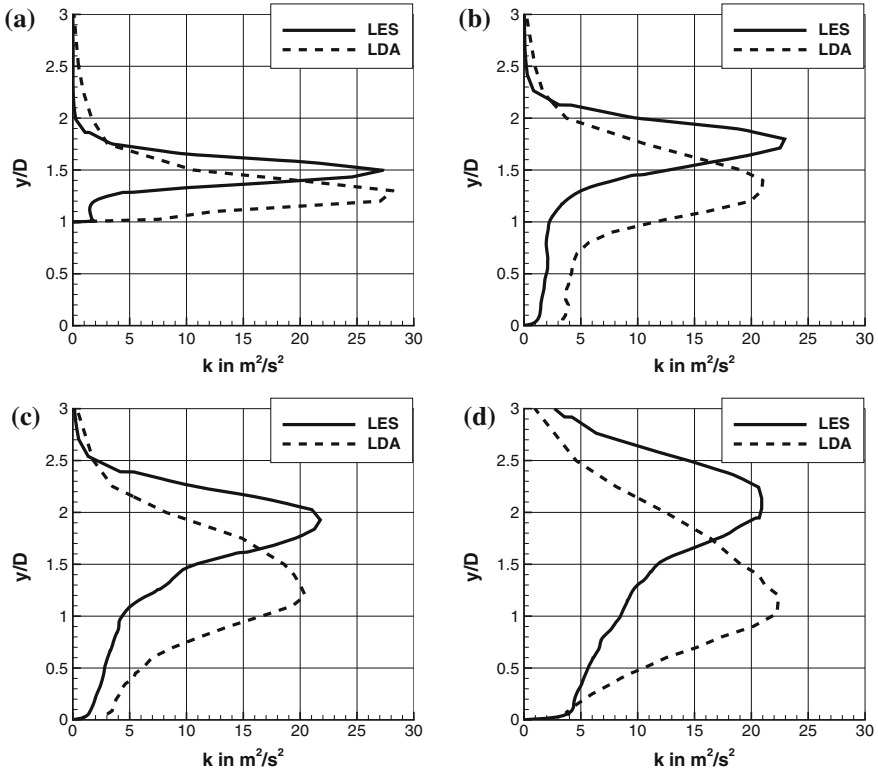


Fig. 4 Comparison of turbulent kinetic energy profiles from LES and LDA-measurements. **a** k-profiles at $x = 0D$ behind step, **b** k-profiles at $x = 1D$ behind step, **c** k-profiles at $x = 2D$ behind step, **d** k-profiles at $x = 4D$ behind step

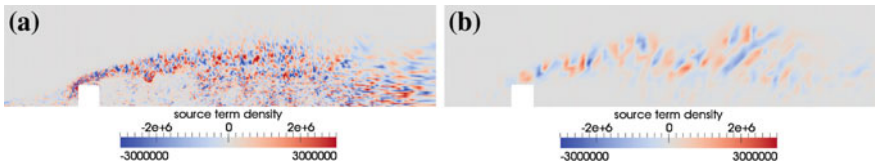


Fig. 5 Acoustic source term density on CFD grid and conservative interpolation on CAA grid. **a** Acoustic source term density on fine CFD grid, **b** interpolated acoustic source term density on coarse CAA grid

sity at a distinct time step on the fine CFD grid, as well as on the much coarser CAA grid is shown. The source term density is created by dividing the source term value by the related cell volumes. The interpolation between the two grids is performed conservatively. The dominant acoustic sources are located in the shear layer of the obstacle's recirculation area. This is the flow region with the largest turbulent fluctuations, which can be seen in the distribution of turbulent kinetic energy (Fig. 3).

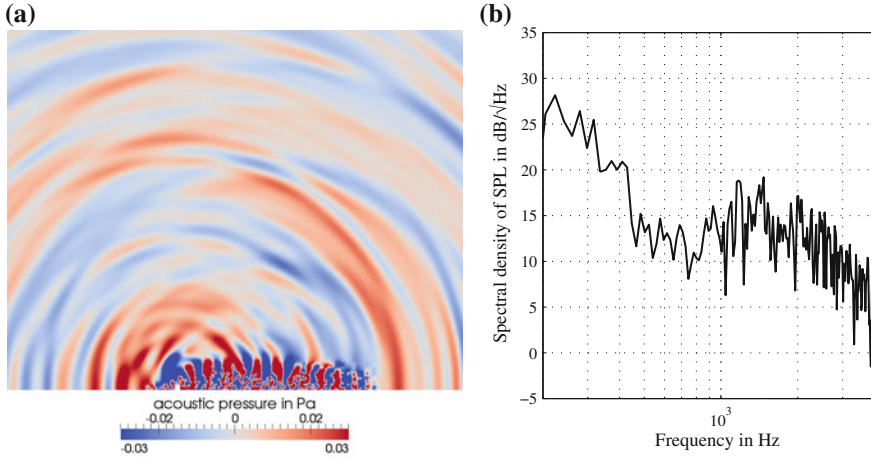


Fig. 6 Acoustic field for 20 m/s. **a** Distribution of acoustic pressure. **b** Power spectral density of sound pressure level (Source point 1 m above obstacle)

The results of the acoustic computation are shown in Fig. 6. The distribution of the acoustic pressure is illustrated in Fig. 6a. Here, one has to consider that Lighthill’s acoustic analogy is not valid in the source region. Only for the propagation region where no source terms are present, pure wave propagation is computed. The power spectral density of the acoustic sound pressure level (SPL) at the monitor point 1 m above the obstacle is plotted in Fig. 6b. The sound radiation is dominated by broadband noise. The maximum of the sound emission lies in a frequency region below 500 Hz. A second maximum can be found in the region between 1000 and 2000 Hz.

4.3 Microphone Measurements and Comparison to Numerical Results

Microphone measurement were conducted in an acoustic wind tunnel under anechoic chamber conditions. Two configurations were investigated. The first configuration was a reference configuration consisting of a flat plate without obstacle. The second configurations is the flat plate with obstacle mounted. The velocities were chosen to be 20 and 30 m/s. In Fig. 7, the results are illustrated. The investigated frequency range starts from 200 Hz. This is the lower frequency limit for the acoustic wind tunnel to assume free field conditions [9]. For the configuration without obstacle, a nearly linear descend of the SPL can be observed. The difference between the two velocities results in a constant offset of approximately 10–12 dB. The effect of the step is mainly visible through an elevation of the SPL between 10³ and 10⁴ Hz.

Fig. 7 Microphone measurement for 20 and 30 m/s

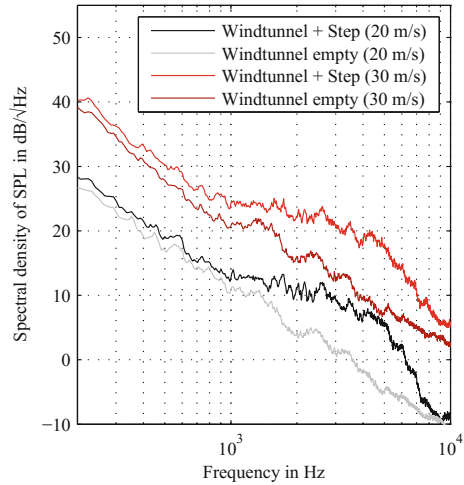


Table 1 Integral values of measured and simulated sound pressure level

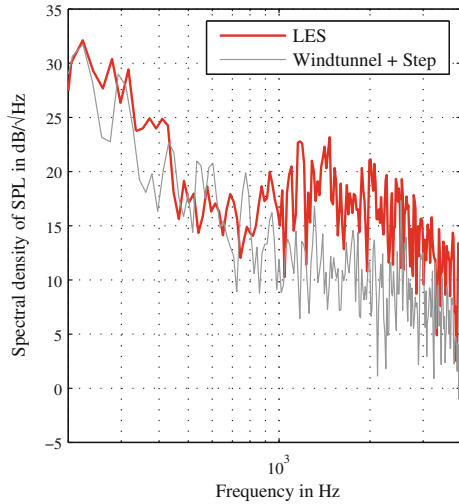
Velocity (m/s)	Wind tunnel empty (dB)	Wind tunnel + step (dB)	Simulation
20	49	51.4	54.9 dB
30	60.3	63.1	

The difference between the configuration including the obstacle and the flat plate is similar for both velocities.

An integral evaluation of the sound pressure level for the illustrated frequency region between 200 and 10⁴ Hz is shown in Table 1. The difference between 20 and 30 m/s is approximately 11 dB. The influence of the step results in a difference of approximately 2–3 dB in sound pressure level.

The comparison between measurements and simulation is given in Fig. 8. Due to temporal and spatial resolution limits of the acoustic simulation, spectral analysis of the signals is performed until 4000 Hz. For the calculation of the integral sound pressure level, the frequency region between 200 and 4000 Hz was used. For comparison reasons, the evaluation of the measured values is equivalent to the simulation data. A time period equal to the simulation time was extracted and downsampled. Due to the difference between the spanwise extent of the simulated geometry (5*D*) and the experimentally investigated geometry (wind tunnel nozzle width 12.48*D*) the simulated results have to be corrected by adding $10 \log N = 10 \log(12.48D/5D) \approx 4$ dB to the spectrum in Fig. 8 [3] (*N* is the ratio of wind tunnel nozzle width to simulated geometry width). Simulation and measurement are in good accordance. Between 200 and 800 Hz, the slope of both signals is equal. The simulation values are in good agreement with the measured data in this region. The influence of the step through a slight elevation of the SPL spectrum is visible in the simulated data as well. In comparison to the measurement it is more distinct and starts at 800 Hz. The SPL

Fig. 8 Comparison between simulation and measurement for 20 m/s (LES data corrected for comparison with wind tunnel data)



spectrum of the simulation data gives values which are approximately 5 dB higher than the measured values for the frequency region influenced through appearance of the step. A possible explanation for the differences is the overestimated extent of the rear recirculation region in the simulation compared to the experiment. The integral evaluation for the illustrated frequency range between 200 and 4000 Hz yields a sound pressure level of 51.4 dB for the measurements and 54.9 dB for the corrected simulation data (Table 1).

5 Summary and Conclusion

Numerical simulations and measurements of the flow field and the resulting acoustical field of a forward-backward facing step are presented. The turbulent flow field is computed with the means of LES. Lighthill's acoustic analogy is used with the second spatial derivative of the pressure field as source term. The distribution of the source terms identifies the shear layer of the rear recirculation area to be mainly responsible for the generation of sound. Additional, experimental investigations of the sound radiation of the forward-backward facing step are presented. The influence of the step compared with a flat plate configuration comes apparent through an elevation of the spectra for frequencies between 10³ and 10⁴ Hz. The numerical results for the acoustical field are in good agreement with the measurements. The spectral distribution of the sound pressure level as well as integral evaluations show only minor deviations.

References

1. Schäfer, F., Müller, S., Uffinger, Th., Becker, S., Grabinger, J.: Fluid-structure-acoustics interaction of the flow past a thin flexible structure. *AIAA J.* **48**(4) (2010)
2. Addad, Y., Laurance, D., Talotte, C., Jacob, M.C.: Large eddy simulation of a forward-backward facing step for acoustic source identification. *Int. J. Heat Fluid Flow* **24**(4), 562–571 (2003)
3. Moon, Y.J., Seo J.H., Bae, Y.M., Roger, M., Becker S.: A hybrid prediction method for low-subsonic turbulent flow noise. *Comput. Fluids* **39**(7), 1125–1135 (2010)
4. Durst, F., Schäfer, M.: A parallel block/structured multigrid method for the prediction of incompressible flows. *Int. J. Numer. Methods Fluids* **22**, 549–565 (1996)
5. Kaltenbacher, M.: Advanced simulation tool for the design of sensors and actuators. *Procedia Engineering*. **5**, 597–600 (2010)
6. Hüppe, A.: Spectral finite elements for acoustic field computation, dissertation, Vienna University of Technology (2012)
7. Esmaeili, A.: Integrated source term calculation of lighthills acoustic analogy for hybrid aeroacoustic computations on parallel computers, master thesis, University Erlangen-Nuremberg (2012)
8. Kaltenbacher, M., Escobar, M., Becker, S., Ali, I.: In: Marburg, S., Nolte, B. (eds.) *Computational Acoustics of Noise Propagation in Fluids. Computational Aeroacoustics Based on Lighthill's Acoustic Analogy*, pp. 115–142. Springer, Berlin (2008)
9. Hahn, C., Becker, S., Ali, I., Escobar, M., Kaltenbacher, M.: Investigation of Flow Induced Sound Radiated by a Forward Facing Step. *New results in numerical and experimental fluid mechanics 6*. Springer, Berlin (2007)